

**Doping-enhanced dipolar dynamics in ice V as a precursor of hydrogen ordering in ice XIII**K. W. Köster,<sup>1</sup> A. Raidt,<sup>1</sup> V. Fuentes Landete,<sup>2</sup> C. Gainaru,<sup>1</sup> T. Loerting,<sup>2</sup> and R. Böhmer<sup>1</sup><sup>1</sup>*Fakultät Physik, Technische Universität Dortmund, D-44221 Dortmund, Germany*<sup>2</sup>*Institute of Physical Chemistry, University of Innsbruck, A-6020 Innsbruck, Austria*

(Received 5 September 2016; published 15 November 2016)

Dielectric spectroscopy measurements are carried out in the temperature range from about 100 to 145 K on nominally pure ice V as well as on crystals doped with KOH and with HCl in order to investigate their reorientation dynamics at ambient pressure. The orientational glass transition temperature of pure ice V is detected at 123 K, in agreement with previous indications from calorimetry. KOH doped ice V displays an about 60-fold enhanced hydrogen dynamics and the dipolar relaxation induced by HCl doping is even by a factor of about 40 000 faster than that of the undoped material. The phase transition of HCl doped ice V to ice XIII is accompanied by a significant reorientational slowdown and a pronounced freeze-out of the electrical susceptibility. The results obtained near this transition are discussed in relation to other order/disorder ice pairs such as ice I/XI and ice XII/XIV.

DOI: [10.1103/PhysRevB.94.184306](https://doi.org/10.1103/PhysRevB.94.184306)**I. INTRODUCTION**

There is only a single substance, H<sub>2</sub>O, for which a total of about 20 distinguishable amorphous [1,2] and crystalline [3–6] modifications is currently known. And the youngest member of the family, crystalline ice XVI [7]—which may be viewed as an empty cubic sII structure clathrate hydrate—is just two years old. On the ice XVI lattice, the water molecules are orientationally disordered at low temperatures, yet except for ice IV and XVI, all experimentally confirmed disordered crystalline ice phases are accompanied by an ordered counterpart, and therefore, the discovery of further ices is anticipated.

With respect to the generation of orientationally ordered ice phases, two groups may be distinguished. On the one hand, ices III and VII can be ordered “spontaneously”, i.e., thermally driven at relatively high temperatures/pressures of 165 K/0.2 GPa [8] and 270 K/3.0 GPa [9], respectively. On the other hand, ices I, V, VI, and XII all undergo their disorder → order phase transition near or below about 120 K only in the presence of various dopants that catalyze the dynamics on the ice lattices. This suggests that the discovery of further ice phases will likely involve suitable doping. However, details concerning the additionally required experimental procedures and so far the specific type of dopant are all but clear [10].

For hexagonal ice (ice I<sub>h</sub>) [11–17] and for related systems such as the sII clathrate hydrates [18–22], it has long been shown that alkali hydroxide doping can lead to a low-temperature orientational ordering [23]. Despite occasional other suggestions [24], dopants such as alkali or hydrogen halides, earth alkali hydroxides, or ammonia are ineffective in catalyzing a hydrogen ordered low-temperature phase [11].

Dielectric measurements revealed that, with respect to undoped ice I<sub>h</sub>, doping with HCl, NH<sub>4</sub>F, and KOH generates enhanced Debye-type dynamics, i.e., close to simple exponential relaxations, called D-2 dispersion in Ref. [25]. Samples with these various dopants display almost indistinguishable time constants which, e.g., at 125 K, are close to about 1 s. However, some dopants give rise to an additional, much faster relaxation process on a time scale  $\tau_f$  which at this temperature is shorter by a factor varying from 10 (in NH<sub>4</sub>F doped ice I<sub>h</sub>) to 10<sup>5</sup> (in KOH doped ice I<sub>h</sub>) [25]. It is only this latter enormous KOH-induced dynamical enhancement and the

eventual slowdown of  $\tau_f$  to about 1 s near temperatures of 75 K which appears instrumental for the ice I<sub>h</sub> → ice XI transition that was first unraveled [11] in 1972 and calorimetrically confirmed later on [15].

Despite the insights inferred from these early observations, transitions to orientationally ordered phases starting from HCl (in some cases HF) doped ice V, VI, and XII as mother phases could be demonstrated experimentally by Salzmann *et al.* only in 2006 and 2009 [5,6]. The consequences of doping with KOH were scrutinized for ice V using a range of experimental methods (predominantly) probing structural [26], calorimetric [27], and vibrational [28] properties. However, based on a careful calorimetric study [29], it became clear that some of the previous hints [28] for an order-disorder transition in KOH-doped (and even in pure [30]) ice V rather reflect *partial* hydrogen ordering only. Ice XIII, the ordered variant of HCl (or HF) doped ice V, was examined by various thermodynamic [29] and spectroscopic experiments [31], as well as by means of theoretical calculations [32] and simulations [33,34].

Undoped ice V has been studied using a wide range of methods including calorimetry [27,29,35,36], rheology [37,38], Brillouin scattering [39], x-ray and neutron diffraction [35,40–42], vibrational spectroscopy [43–47], as well as computer simulation [33,48,49]. Using dielectric spectroscopy, the main method employed in this paper, ice V devoid of ionic doping [50] was so far investigated in the pressure region of 0.35 to 0.64 GPa [30,51,52]. Conversely, with a focus on exploring dynamical aspects leading to the ice V → ice XIII phase transition, here we report on the ambient-pressure dipolar response not only of undoped ice V but also of KOH and HCl doped crystals.

This paper complements a recent experimental study of pure and doped ice XII [53]. For this high-pressure generated ice, HCl doping leads to the formation of ice XIV, a hydrogen ordered phase [5]. Furthermore, we will compare the doping-induced dynamic enhancement for the ice V system with literature data on doped ice I<sub>h</sub>, ice XII, and clathrate hydrates.

**II. EXPERIMENTAL DETAILS**

For the present work, the ices were prepared with D<sub>2</sub>O obtained from Sigma-Aldrich (99.9% D) and ultrapure H<sub>2</sub>O

(80 M $\Omega$ ) in a piston-cylinder setup as follows: 600  $\mu$ L of water (or 0.01 M solutions of the specified dopants) were pipetted into an indium container and pushed into the 8 mm bore of the cylinder which is kept at 77 K. The ice frozen this way was then compressed to 0.5 GPa and heated through a series of polymorphic phase transitions, resulting ultimately in ice V at 250 K [29]. The ice V samples were then cooled to 77 K. Below about 110 K, the transformation to ice XIII takes place if the ice is HCl (DCl) doped. In all other cases, no phase transitions are experienced upon cooling. After pressure release and recovery of the ices at 77 K, they were characterized by means of calorimetry and x-ray diffraction.

Homogeneity and purity of the ice V samples prepared this way were checked using powder x-ray diffraction in a Siemens D5000 instrument using Cu-K $\alpha$  radiation (1.5406 Å). To this end, the quench-recovered samples were transferred to an Anton-Paar TTK450 cryochamber which features a flat-plate sample holder (made of nickel plated copper) to study samples in  $\theta$ - $\theta$  geometry. While immersed in liquid nitrogen, the sample is powdered. Then it is placed on a spoon, moved through a short distance of ambient air, and placed onto the sample holder that was precooled to  $\approx$ 80 K. Immediately thereafter, the chamber is closed and evacuated to less than 1 mbar. A small amount of hexagonal ice may condense onto the sample during this procedure, which is marked by the dashed vertical lines in Fig. 1. Nickel and copper Bragg peaks stemming from the sample holder are marked by solid vertical lines. The other Bragg peaks match with literature data [42] for ice V which are shown as tick marks at the bottom of Fig. 1. For HCl doping (ice XIII), one recognizes a weak Bragg peak at  $2\theta = 32.2^\circ$  indicative for hydrogen ordering. For DCl doping, no clear Bragg peak is discernible at this angle, making it hard to judge the degree of ordering in this sample from these experiments. At  $32.2^\circ$  a peak is definitely absent in all other diffractograms, i.e., there are no signs of hydrogen ordering for the undoped or KOH-doped samples. The x-ray diffractograms do not show any unexplained Bragg peaks for any of the samples. This demonstrates that the presence of dopant or deuterium does not affect the sample purity. The homogeneity of the cylindrical samples was tested by taking pieces from different parts of the cylinder and conducting additional runs. There is a perfect match of all recorded diffractograms, i.e., the samples are fully homogeneous. The only difference between different diffractograms is the different intensity of individual Bragg peaks. This is caused by preferred orientation effects (texture) of powder grains on the flat sample holder and cannot be avoided in  $\theta$ - $\theta$  geometry, i.e., without rotating the sample in all directions. Texture effects are well recognized when inspecting the diffractogram recorded for ice V from pure H<sub>2</sub>O in Fig. 1 (middle). At  $2\theta \approx 28$ – $35^\circ$ , its intensity pattern differs from that of the other samples. This difference regarding the intense Bragg peaks is related to differences in grain size and the amount of sample on the holder, which is less for ice V from pure H<sub>2</sub>O. Therefore, also the Bragg peaks originating from the sample holder are more prominent.

After preparation and characterization in Innsbruck, the 77 K cold samples were shipped to Dortmund, powdered, and transferred to a parallel-plate capacitor made of invar

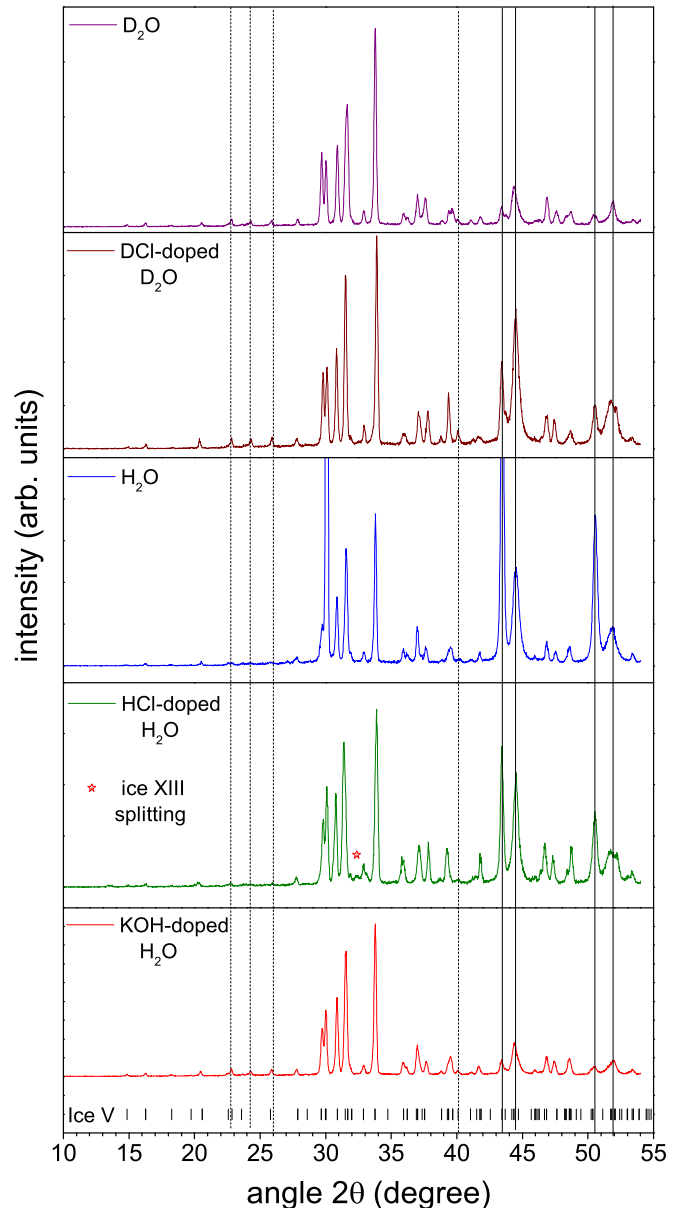


FIG. 1. X-ray diffractograms of doped and/or deuterium labeled ice V/XIII samples recorded at 80 K and  $<1$  mbar after quench recovery and powdering in liquid nitrogen. Vertical dotted and solid lines mark positions of Bragg peaks caused by traces of ice I<sub>h</sub> and the sample holder (Ni/Cu), respectively. The asterisk marks the (31 $\bar{2}$ ) Bragg peak of ice XIII.

and sapphire [54]. The whole procedure was performed at liquid nitrogen temperature. The cell was inserted in a cryostat precooled to about 95 K, and broadband dielectric spectra were acquired at ambient pressure with an Alpha analyzer after the temperature was stabilized within 0.2 K by a Quatro controller, both devices being incorporated in a turnkey system from Novocontrol. For a typical scan ranging down to  $2 \times 10^{-2}$  Hz, the effective heating and cooling rates were 0.1 K/min. Due to uncertainties of the filling factor, the dielectric losses are presented in arbitrary units.

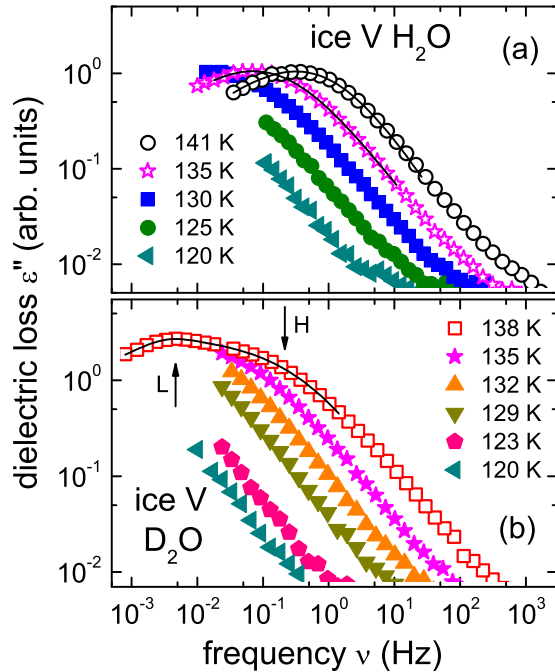


FIG. 2. Temperature-dependent dielectric loss of (a) protonated and (b) deuterated ice V. The solid lines represent fits using Eq. (1) in panel (a) and a variant of Eq. (1) including two relaxation processes in panel (b). The ratio of time scales for the relaxation processes in (b) at high frequency (index H, visible as a shoulder) and low frequency (index L, visible as a peak) is  $\tau_L/\tau_H = 12 \pm 3$ . The frequencies of the two contributions are marked by arrows.

### III. RESULTS AND ANALYSES

#### A. Pure and doped ice V

In Fig. 2(a), dielectric loss spectra of undoped  $\text{H}_2\text{O}$  ice V are shown for several temperatures. One recognizes that well-defined loss peaks shift through the experimentally accessible frequency window as the hydrogen dynamics slow down upon cooling. To describe the loss spectra in a quantitative fashion, the Havriliak-Negami function combined with a power-law accounting for the conductivity contribution

$$\varepsilon''(\nu) = \Delta\varepsilon \text{Im}\{[1 + (2\pi i\nu\tau)^\alpha]^{-\gamma}\} + A\nu^{-B}, \quad (1)$$

was used. Here, the loss peak is characterized by a relaxation strength  $\Delta\varepsilon$  and by the shape parameters  $\alpha$  and  $\gamma$  that account for the width and asymmetry of the distribution of time scales  $\tau$ . The description of the conductivity involves two variables, the prefactor  $A$  and the exponent  $B$ . The solid lines in Fig. 2(a) represent fits using Eq. (1) and show that the spectral width is independent of temperature. The relaxation strength  $\Delta\varepsilon$  varies by only 5% in the accessible  $T$  range. The relaxation times  $\tau$  emerging from this analysis turned out to evolve in a thermally activated fashion. They are discussed in Sec. IV below.

The temperature range in which dielectric loss peaks can be resolved from the data in Fig. 2 and thus relaxation times can be extracted directly is confined to a window which, on the high-temperature side, is limited by the incipient phase transition to cubic ice (occurring when the peak frequency reaches about 1 Hz). Towards low temperatures, frequency-temperature equivalence (FTE) can be exploited to overcome

some limitations imposed by the accessible frequency range. To this end, it is useful to plot the dielectric loss spectra in a double logarithmic fashion as done in Fig. 2. Here, one immediately recognizes that the power-law behavior of the high-frequency flank of  $\varepsilon''$ , as implied by Eq. (1), is independent of temperature. This observation is a prerequisite for the applicability of FTE which allows one to construct a master curve by shifting the loss spectra along the frequency axis until the data superimpose. From the necessary shift factors, the otherwise inaccessible peak frequencies can be assessed.

This procedure is useful also for analyzing the spectra for undoped  $\text{D}_2\text{O}$  ice V, see Fig. 2(b). Overall, from Fig. 2, one recognizes that the dynamics in the deuterated sample are slower than in the protonated one. This finding underscores the relevance of isotope effects that show up for various crystalline [55–57] and amorphous [58] ice phases.

Furthermore, the peak region of  $\text{D}_2\text{O}$  ice V is much broader than that of the protonated ice. In fact, while the data for  $\text{H}_2\text{O}$  ice V can be parameterized using a single relaxation process, for  $\text{D}_2\text{O}$  ice V, a fit using two relaxation contributions describes the data significantly better. The high-frequency contribution, marked H in Fig. 2(b), has reduced relaxation strength and is visible as a shoulder in  $\varepsilon''(\omega)$ . The microscopic reason for the occurrence of *two* contributions is unclear.

Very broad loss peaks plus a significant electrical conductivity contribution may sometimes obscure the low-frequency part of the loss peaks for samples in which doping generates ionic species. The data of KOH-doped ice V, shown in Fig. 3(b), are an example for this situation. One can see that, again, the high-frequency flank of the curves is independent of temperature so that the evolution of the thermally active dynamics can be traced over a large range, see also Sec. IV below. By inspecting the data in Fig. 3, it is clear that KOH doping enhances the dipolar dynamics in ice V by almost two orders of magnitude, see the arrows in Fig. 3 that mark the peak frequencies of the spectra recorded at about 135 K.

An even more dramatic dynamical enhancement is caused by the addition of HCl to ice V. This is evident from the dielectric loss spectra summarized in Fig. 3(c). Here, as the arrows indicate, doping shortens the time scale by a factor of about 40 000 with respect to that in pure ice V.

The “acceleration factor” of about  $10^4$  that characterizes the most effective dopant (HCl) is only slightly smaller than those reported for the catalysts generating the largest dynamical effects in ice  $\text{I}_h(\text{KOH})$  Ref. [25] and ice  $\text{XII}(\text{HCl})$  Ref. [53], which were found to eventually lead to the ordered phases ice XI and ice XIV, respectively. Hence, monitoring the dielectric response of ice V(HCl) down to lower temperatures allowed us to study the ordering transition in this ice phase, as will be demonstrated in the following.

#### B. The ice V $\leftrightarrow$ ice XIII phase transition

In Fig. 4, we summarize the dielectric loss spectra that were recorded for HCl-doped  $\text{H}_2\text{O}$  ice XIII/ice V. Frame (a) shows that, upon heating the sample from 108 to beyond 120 K, the dielectric loss peak amplitudes increase significantly and most steeply at about 114 K. In addition, the well-defined loss peaks display the strongest frequency shift near this temperature.

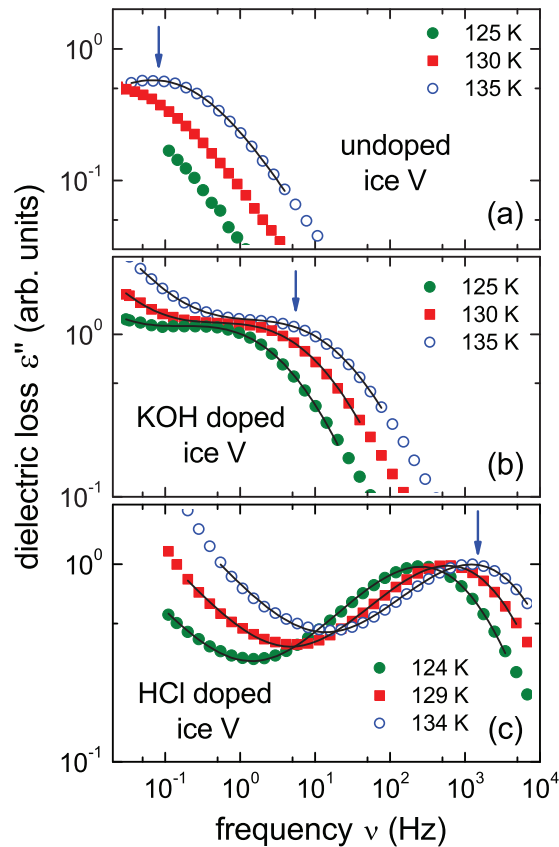


FIG. 3. Double logarithmic plot of the temperature-dependent dielectric loss of (a) undoped, (b) KOH-doped, and (c) HCl-doped protonated ice V. The arrows highlight the time scale difference observed at 134–135 K. Solid lines are fits using Eq. (1).

This obviously indicates the transition from ice XIII to ice V. Upon subsequent cooling, very similar results are obtained, see Fig. 4(b), confirming that the ice V  $\leftrightarrow$  ice XIII transition is fully reversible at ambient pressure [29], despite the fact that both phases require the application of pressures in excess of 0.5 GPa for their initial production.

As shown in Fig. 5, similar results were obtained for DCI-doped D<sub>2</sub>O ice XIII/ice V. One recognizes though that its dynamics are somewhat slower than in the protonated analog, cf. Fig. 4: The dynamics in the samples produced from heavy water are a factor of 10 slower than in their protonated counterparts.

Furthermore, the decrease of the dielectric loss peak observed upon cooling, compare Fig. 5(a) with Fig. 4(a), displays a clear isotope effect. To characterize the ice V  $\leftrightarrow$  ice XIII transition quantitatively, we determined the dielectric loss peak amplitude  $\varepsilon''_{\max}$  from the heating as well as from the cooling runs shown in Figs. 4 and 5. The results are presented in Fig. 6. For the protonated samples, they indicate an about two thirds reduction of the static susceptibility as a consequence of the ordering transition that obviously immobilizes the hydrogen dynamics on the ice lattice. Figure 6 illustrates directly that  $\varepsilon''_{\max}$  varies most steeply near 114 K in both the upscan and the subsequent downscan.

For the deuterated sample, Fig. 6 shows that the transition-related reduction of the loss peak amplitude is rather small.

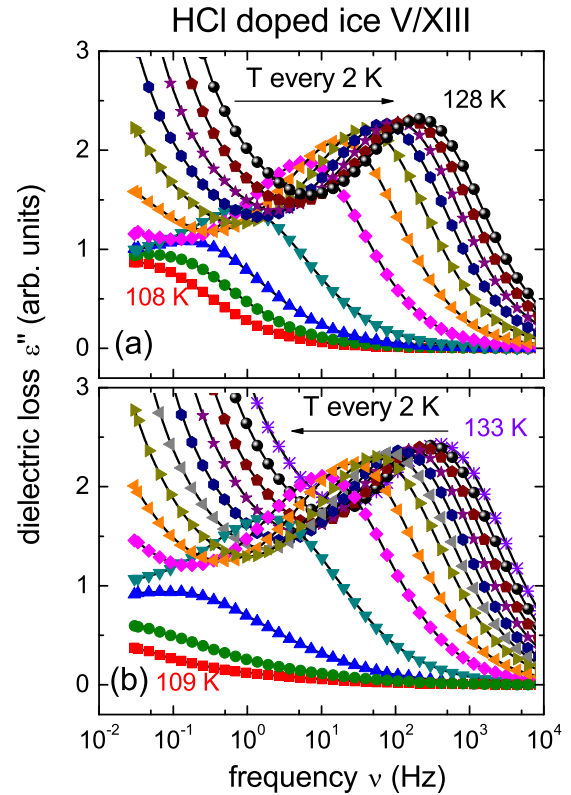


FIG. 4. Dielectric loss spectra of protonated ice V/XIII doped with HCl as measured in steps of 2 K while (a) heating or (b) cooling the sample with an average rate of 0.1 K/min. Towards low temperatures, the dielectric loss signals a significant reduction of the static dipolar susceptibility as a consequence of hydrogen ordering.

For both isotopomers, only a weak hysteretic behavior is discernible, and together with the continuous thermal evolution of the relaxation strength,  $\varepsilon''_{\max}(T)$  suggests a transition which is weakly first order. Indications for the two-stage transition observed in Ref. [31], where it was noted “that it is more complicated than a simple first-order transition,” could not be resolved. For comparison, a more pronounced hysteretic behavior was noted from powder neutron diffraction experiments at cooling and heating rates of 0.2 K min<sup>-1</sup> [59]: Onset temperatures of 108 K upon heating and 117 K upon cooling were inferred from the change in lattice parameters for DCI-doped D<sub>2</sub>O samples. Interestingly, the lattice parameters change by less than 1% at the ice V  $\leftrightarrow$  ice XIII transition. Here, for the dielectric susceptibility, we find a change of about 15% in Fig. 6 for DCI doping and even 70% for HCl doping. A pronounced hysteresis for the ice V  $\leftrightarrow$  ice XIII transition was observed for DCI-doped D<sub>2</sub>O samples in calorimetric experiments, which reveal onsets of 108 and 117 K for heating and cooling at 5 K min<sup>-1</sup>, respectively [29].

At first glance, the large isotope difference in the evolution of the susceptibility for  $T < T_c$  may seem surprising. However, when comparing with results of alkali hydroxide-doped ice I<sub>h</sub>, a similar pattern is found, see the inset in Fig. 6. These data demonstrate that the susceptibility reduction in the deuterated ice is only about 15% of that of the protonated KOH doped ice. We interpret these differences to indicate that the order

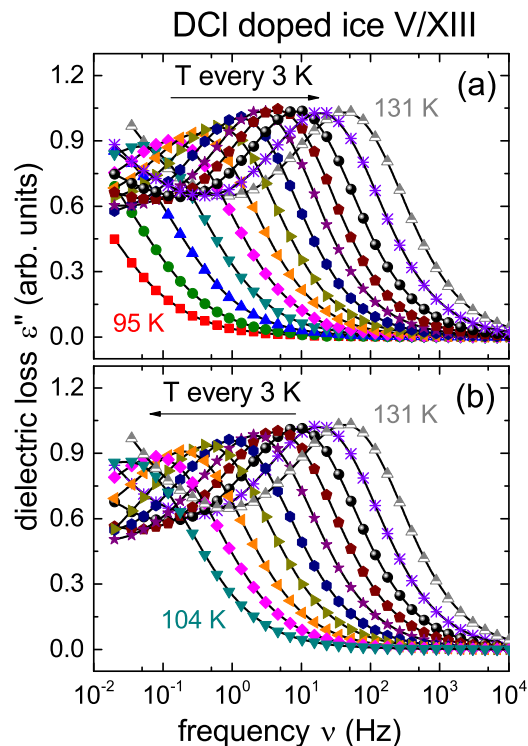


FIG. 5. Dielectric loss spectra of deuterated ice V/XIII doped with DCI as measured while (a) heating or (b) cooling the sample. Towards low temperatures, the dielectric loss reduction is less pronounced than in the protonated analog.

parameter achieved in the investigated protonated ices is significantly higher than those in the deuterated ones.

Even though it cannot be ruled out that, for the protonated sample, the relative relaxation strength would drop to values much below one third upon cooling to temperatures much below 100 K, the low-temperature value of  $\epsilon''_{\max}$  even of  $\text{H}_2\text{O}$  ice V seems to be finite. It is worthwhile to recall that neutron diffraction studies on ice V recovered to ambient pressure revealed that this ice phase is not completely orientationally disordered [41,42] and that ice XIII retains a small degree of disorder [5]. Hence, a complete change of the order parameter from 0 to 100% is not anticipated. Indeed, in calorimetric studies [29], the entropy change detected at the ice XIII  $\leftrightarrow$  V transition was found to be 66% of that expected for a transition from complete orientational order to complete orientational disorder. Ice V features 28 molecules in the unit cell of its complex monoclinic crystal structure, and some proton sites display a larger occupation probability than others [59] so that “the factors responsible for the partial order cannot be easily identified for such a complicated structure” as Lobban *et al.* have put it [42].

#### IV. DISCUSSION

##### A. Relaxation times of ice V and ice XIII

The time scales  $\tau$  dielectrically determined for doped ice V, for undoped ice V, and for ice XIII(HCl) are summarized in Fig. 7. This Arrhenius plot includes data obtained either from the frequency of the loss peak maximum  $\nu_{\max}$  via

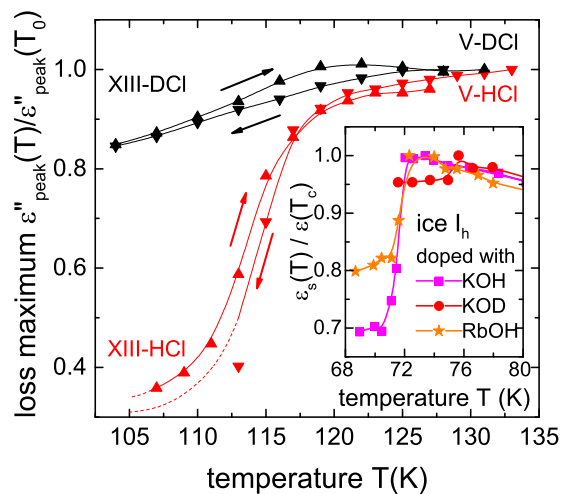


FIG. 6. Dielectric loss peak amplitudes  $\epsilon''_{\max}$  of ice V/XIII as determined from cooling and heating runs. The peak amplitudes are normalized to their high-temperature values. The solid lines are drawn to guide the eye, and the arrows indicate the direction of temperature change. The inset shows the temperature dependence of the static susceptibility  $\epsilon_s$  of ice I taken from the work of Kawada *et al.* The data are normalized to their value  $\epsilon(T_c)$ , which is 501 for KOH- [13], 474 for KOD- [16], and 431 for RbOH-doped [14] ice  $I_h$ .

$\tau = (2\pi\nu_{\max})^{-1}$  using Eq. (1) (full symbols) or from the frequency scaling based on FTE (see Sec. III A, open symbols). In Fig. 7, the time scales are seen to follow thermally activated behavior that can be described by

$$\tau = \tau_0 \exp(E/RT), \quad (2)$$

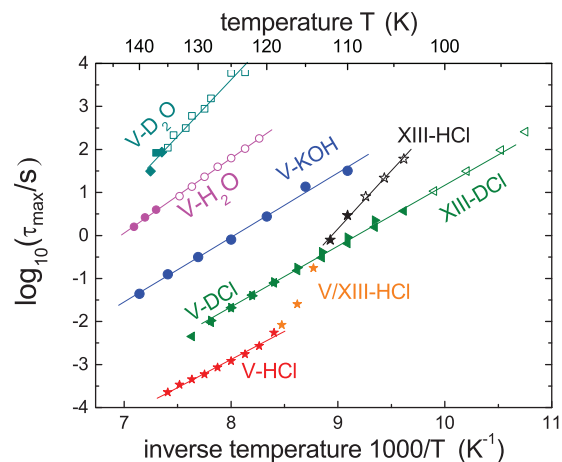


FIG. 7. Arrhenius representation of the time scales  $\tau_{\max} = \tau$  of undoped and KOH-doped  $\text{H}_2\text{O}$  ice V as well as of HCl-doped ice V/XIII. Data for deuterated undoped ice V (relating to the peak designated L in Fig. 2) and DCI-doped deuterated ice V/XIII are also shown. We note that, for the latter system, a measurement from a different batch yielded time constants that were a factor of 4.2 longer than those shown in the figure. It is interesting to observe that HCl-doped  $\text{H}_2\text{O}$  ice V/XIII displays an enormous change of time scale near the order-disorder transition, while DCI-doped  $\text{D}_2\text{O}$  ice V/XIII follows the same Arrhenius dependence, Eq. (2), over the entire range. The energy barriers corresponding to the solid lines are given in Table I.

where  $\tau_0$  is a preexponential factor. From that figure, one recognizes the large time scale separations already inferrable from the dielectric spectra shown in Fig. 3, but also that pure ice V exhibits a slightly larger energy barrier ( $34 \pm 2$  kJ/mol) than HCl-doped ice V ( $23 \pm 2$  kJ/mol). Interestingly, in the temperature regime of the ice V  $\leftrightarrow$  ice XIII transition, the relaxation times vary much stronger, and in the low-temperature phase, an energy barrier of  $52 \pm 4$  kJ/mol is observed. This latter finding makes sense since suitable doping facilitates the dynamics and is thus expected to reduce the effective energy barrier, while in the ordered phase, motion becomes increasingly impeded. From Fig. 7, one recognizes that, for ice V, the energy barriers of HCl-doped H<sub>2</sub>O and DCl-doped D<sub>2</sub>O ice are similar, but surprisingly, for undoped ice V, a large isotope difference shows up (H<sub>2</sub>O ice V:  $E = 34 \pm 2$  kJ/mol; D<sub>2</sub>O ice V:  $E = 51 \pm 4$  kJ/mol).

The slowdown and eventual arrest of the hydrogen dynamics on the experimental time scale is indicative for the occurrence of an orientational glass transition in pure and KOH-doped ice V. Such a transition is known for pure ice V from previous calorimetric studies to occur at an onset temperature  $T_{\text{onset}}$  of about  $123 \pm 3$  K [27,36], which is the temperature at which the dielectric time scale is 100 s, cf. Fig. 7 [60]. In this context, it is worthwhile to point out that, in general, calorimetric onset temperatures measured for scan rates of the order of 10 K/min correspond to typical structural or dielectric relaxation times roughly near 100 s [61].

Based on this 100 s criterion for the dielectric relaxation time, an orientational glass transition temperature of 106 K is expected for ice V(KOH). Indeed curves (3) to (5) in Fig. 7 of Ref. [29], which refer to heating scans at rates of 1 to 30 K min<sup>-1</sup>, indicate calorimetric glass transitions near this temperature.

For ice XIII(HCl), the present dielectric data show that a dipolar time scale of 100 s is reached at 103 K, cf. Fig. 7. This latter value roughly corresponds to the temperature of about 105 K at which kinetic unfreezing was calorimetrically observed to commence in acid-doped ice XIII upon heating [29]. This temperature can be compared with the “extrapolated peak onset temperatures of the endothermic peaks on heating” of  $T_e = 110$  K inferred from differential scanning calorimetry (DSC) of the phase transition [29].

In Ref. [29], it was stated that “KOH doping of ice V . . . does not induce sufficient orientational ordering to cause a phase transition to ordered ice XIII,” yet as Fig. 7 shows, the dynamics of ice V(KOH) are just a factor of about 50 slower than that of deuterated ice V(DCl), which displays a  $T_e$  of 108 K [62]. Hence, also from the present dielectric data, it appears that KOH doping of ice V produces a material which is just at the verge of becoming ordered. In fact, based on calorimetric evidence, ice V(KOH) was initially believed to undergo an order/disorder phase change [27].

Apart from the isotope effect on the time scale of hydrogen chloride-doped ice V ( $\tau$  in the deuterated sample is a factor of about 20 slower than in the protonated one), a striking difference in behavior shows up near the ice V  $\rightarrow$  XIII phase transition, cf. Fig. 7: While ice V(HCl) displays a precipitous change of the observable time scale, for ice V(DCl) a dynamic signature of the transition is not discernible. This circumstance leads to an effective crossing of time scale and to

the remarkable finding of slower hydrogen dynamics in H<sub>2</sub>O ice XIII than in D<sub>2</sub>O ice XIII. Clearly, these effects are counter to what one may have expected.

The inability of our dielectric measurements to detect a hint in the dynamic at the D<sub>2</sub>O ice V  $\rightarrow$  XIII phase transition is to be contrasted with a large degree of similarity in the calorimetric signature of that transition in protonated and deuterated samples. The experiments reported in Ref. [29] reveal comparable transformation enthalpies which are 230 and 200 J/mol for the protonated and deuterated crystals, respectively, both referring to a transition temperature of 112 K. It is noteworthy that it is this temperature at which the dielectric time scales ( $\approx 0.2$  s) of the two crystals are crossing.

We have seen that the relaxation strength of both isotopomers decreases below their respective order/disorder phase transition, but much less so for deuterated ice, cf. Fig. 6. Therefore, it is plausible to assume that, for ice V(DCl) also, the dynamical changes are less pronounced across the order/disorder transition of ice V/XIII, which will be put in a broader context in the next subsection.

## B. Time scales compared with other doped ices

As surprising as the absence of a dynamic signature of the ice V/XIII transition in the deuterated crystals may seem—while in protonated crystals such a dielectric signature is clearly visible—it is not without precedent: A similar finding was reported to occur for potassium hydroxide-doped hexagonal ice when undergoing its phase transition to ice XI, cf. Fig. 8 [16,63]: For H<sub>2</sub>O ice I<sub>h</sub>(KOH), a steplike increase of  $\tau$  by a factor of 32 is observed when cooling the crystal to temperatures below the phase transition, and the energy barrier more than doubles. However, for D<sub>2</sub>O ice I<sub>h</sub>(KOD),  $\tau$  is continuous near the phase transition, and the energy barrier remains almost constant, see Fig. 8.

It is tempting to assume that this minor variation is related to the near absence of a change in the dielectric relaxation strength of KOD-doped D<sub>2</sub>O ice I<sub>h</sub> [16], see the inset of Fig. 6. In other words, the minor 5% drop in the dielectric relaxation strength signals either that, near  $T_c$ , the ability of each of the dipole moments to react to the external electrical field is affected only very little near the ordering transition, or that only few of them effectively freeze out.

In DCl-doped D<sub>2</sub>O ice V/XIII, Fig. 6 shows that, near the transition, the relaxation strength changes by about 15%. Hence, an absence of a dynamic signature in the mean relaxation time could be rationalized by assuming that, below  $T_c$ , a significant relaxation time distribution among the dipolar species emerges and that the slowest of them, which in fact do order, cease to contribute to the dielectric relaxation at all. In this scenario, only the faster, less affected or unaffected degrees of freedom would dominate the relaxation peak. One of the preconditions for this argument to be valid is that, below  $T_c$ , a distribution of relaxation times is indeed present. Inspecting Fig. 4, one recognizes that, for H<sub>2</sub>O ice XIII, a broadened low-frequency flank in  $\epsilon''$  develops below  $T_c$ . While this observation lends some credibility to the suggested interpretation, it has to be admitted that, for D<sub>2</sub>O ice XIII, the situation is not as clear. Here, electrical conductivity effects remain relatively strong down to the lowest temperatures

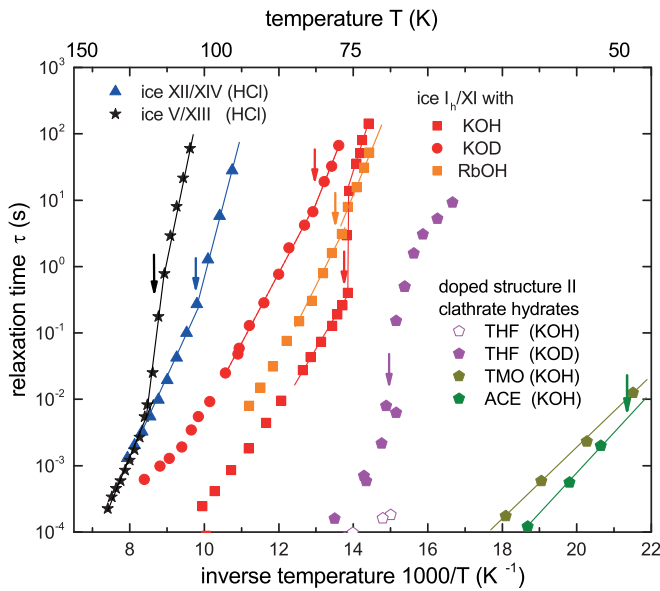


FIG. 8. Comparison of the relaxation times of different doped hydrogen disordered/ordered ice or clathrate hydrate couples. The notation of a protonated or deuterated dopant is meant to imply the protonation or deuteration of the ice or hydrate lattice as well. This figure contains data on KOH-doped ice  $I_h/XI$  [64,65], KOD-doped ice  $I_h/XI$  [16], RbOH-doped ice  $I_h/XI$  [14], HCl-doped ice V/XIII from this paper, and HCl-doped ice XII/XIV [53]. The data on the potassium hydroxide doped clathrate hydrates refer to the guest molecules THF (tetrahydrofuran, doped with KOH [18,70] or KOD [20]), ACE (acetone, with KOH) [21], or TMO (trimethylene oxide, with KOH) [21]. The arrows indicate the phase transition temperatures. The one for the TMO clathrate hydrate (at 34.5 K) is not shown. The solid lines represent Arrhenius laws, cf. Eq. (2).

measured and thus obscure the low-frequency flank of the loss peak.

Now entering a broader discussion of the currently studied ices in comparison with hexagonal ice, let us note that, from studies of the latter, it has long been clear that a

doping-induced transition to ice XI can only be enabled by the alkali hydroxides KOH and RbOH, but not by other dopants, such as NaOH, HF, KF,  $NH_4F$ , or  $Ba(OH)_2$  [11,24,66]. Among the alkali hydroxides, KOH is the most efficient both in terms of enhancing the dynamics (see Table I) and as well as in terms of the entropy change [67] triggered near the phase transition. While entropy and relaxation time depend on doping, it hardly affects the temperature of the ice  $I_h \leftrightarrow$  ice XI phase transition [14]. Substitution of protons by deuterons, however, does shift the temperature from 72 to 76 K, and at 76 K, the relaxation times in potassium hydroxide-doped samples increase about 150-fold, i.e., they increase from 0.08 s ( $H_2O$ ) to 19 s ( $D_2O$ ), cf. Fig. 8 [16,63].

In order to facilitate a survey of the (dielectric) relaxation times in various doped ices, Fig. 8 compiles literature data for ice  $I_h/XI$  and compares them with results for ice XII/XIV from Ref. [53] and ice V/XIII from the present paper in the form of an Arrhenius plot. Table I further summarizes parameters like activation energy  $E$ , phase transition temperature  $T_c$ , and relaxation time  $\tau$ , measured just above and below  $T_c$ . The table also includes data on various KOH-doped clathrate hydrates, which at high temperatures crystallize in the cubic structure sII and which can display (at least partial) proton ordering at low temperatures when containing tetrahydrofuran (THF) [69–72], acetone (ACE), or trimethylene oxide (TMO) as guests [18–22]. These clathrates may currently be considered as closest reference systems for an empty structure sII clathrate hydrate, i.e., for ice XVI for which a hydrogen ordered companion phase was not observed experimentally so far [7].

Interestingly, Fig. 8 shows that the hydrogen ordering phase transitions occur when the (dielectric) relaxation times are typically in the range from 0.01 s (or about 0.001 s if the clathrate hydrates are included) to 100 s, but the relaxation time at  $T_c$  can be much shorter, as exemplified for the  $H_2O$  ice VII  $\leftrightarrow$  ice VIII transition: In the absence of doping, this transition occurs at 2.3 GPa when  $\tau \approx 0.6 \cdot \cdot \cdot 1 \mu s$ , although in ice VII (i.e., for  $T > 271$  K), a relatively large energy barrier of 56 kJ/mol has been reported [73]. Thus, it is not possible

TABLE I. Compilation of energy barriers, phase transition temperatures, and time scales of doped ices and clathrate hydrates. The notation of a protonation or deuteration of the dopant is meant to imply also that of the ice or hydrate lattice in which the dopant is embedded. A bar indicates that this quantity does not exist or could not reliably be determined. A star indicates calculations based on the data at hand or extrapolations of dielectric results to the calorimetric  $T_c$ .

Ice	$E(T > T_c)$ (kJ/mol)	$E(T < T_c)$ (kJ/mol)	$T_c$ (K)	$\tau$ (s) at $T_c$
$I_h$ (LiOH) [17]	14.5	–	–	–
$I_h$ (NaOH) [17]	14.5	–	72 [12]	–
$I_h$ (KOH) $\leftrightarrow$ XI [64,65]	17	35	72 [15,68]	0.4–20
$I_h$ (KOD) $\leftrightarrow$ XI [16]	20	20*	76	27*
$I_h$ (RbOH) $\leftrightarrow$ XI [14,17]	15	15	73 [14]	4–7
V(HCl) $\leftrightarrow$ XIII	$23 \pm 2$	$52 \pm 4$	$113 \pm 4$	0.09–0.16
V(DCl) $\leftrightarrow$ XIII	$28 \pm 2$	–	112 [29]	–
XII(HCl) $\leftrightarrow$ XIV [53]	$21 \pm 2$	$36 \pm 3$	$102 \pm 4$	0.05–0.15
sII clathrate hydrates				
THF(KOH) [18,19]	7.4	–	61.9	0.0006*
THF(KOD) [20]	7.4	–	$67 \pm 4$	0.008–0.5
acetone(KOH) [21]	8.5	–	46.6	0.001–0.2*
TMO(KOH) [21]	9.0	–	34.5	30–300*

to identify a well-defined relaxation time at which an order-disorder phase transition is expected.

While fast dipolar relaxation seems to be a necessary condition for the occurrence of thermally driven [74] hydrogen-ordering phase transitions in the ices, this condition is not sufficient as the case of KOH-doped ice V suggests. Here, doping leads to relaxation times in the range specified above at the ordering temperatures (of the HCl doped samples), yet a phase transformation is not induced. An analogous situation is encountered for HF ice XII (here again referring to the dynamics near the ordering temperature of the HCl doped sample) [53].

Let us finally turn to those KOH-doped clathrate hydrates, which have been reported to undergo a phase transition into a low-temperature proton-ordered state. Here, incorporation of guest molecule reduces  $T_c$  to values significantly below those in KOH-doped ice I (see Table I). It is remarkable that the phase transition temperatures of the doped clathrate hydrates summarized in Table I are all (much) lower than those in the ices. This finding suggests that these clathrate hydrates contain a larger number of dynamics-enhancing defects than the ices. Molecular dynamics simulations have shown that host-guest hydrogen bonds from THF's ether oxygen to adjacent protons on the hydrate lattice can form [75]. This effect reduces the effective proton density on the hydrate lattice and may be viewed as an introduction of Bjerrum L defects in addition to the L (and  $\text{OH}^-$ ) defects caused by KOH doping. These additional L defects [76] obviously enhance the dynamics on the hydrate lattice of clathrates more than in the absence of suitable ether oxygens, see e.g., Fig. 8.

## V. CONCLUSIONS

This paper reports on a dielectric investigation of the dynamics in pure ice V, KOH-doped ice V, and HCl-doped ice V/XIII. We find that addition of KOH leads to a strong ( $\sim 2$  decades) and of HCl to a massive ( $\sim 4.5$  decades) enhancement of the dipolar relaxation rate. Hence, in accord with previous studies on hexagonal ice and on ice XII, the strongest dynamic

speed-up is found for those impurity species that trigger low-temperature proton ordering. In its protonated form, ice XIII displays a strong ( $\sim 70\%$ ) and its deuterated form a moderate ( $\sim 15\%$ ) decrease of the relaxation strength in the studied temperature range. In addition, when comparing the energy barrier  $E$  against dipolar reorientation in  $\text{H}_2\text{O}$  ice V with that in ice XIII, an approximate doubling is found. However, for the deuterated sample, a significant change of  $E$  is not discernible. This behavior resembles that of KOH-doped ice  $\text{I}_h$  where, for the  $\text{H}_2\text{O}$  variant,  $E$  becomes larger by about a factor of two when entering the hydrogen ordered ice XI phase, while for the  $\text{D}_2\text{O}$  variant, there is no significant change. Similarly, the reduction of the static response below the hydrogen ordering phase transition temperature of hydrogen chloride-doped ice V displays a pronounced isotope effect as well. These results are in harmony with analogous ones for potassium hydroxide-doped hexagonal ice, as reported by Kawada *et al* [16,64,65]. The observation of isotope effects calls for particular attention, e.g., when investigating phase transitions in ices with techniques requiring isotope labeling such as deuterium magnetic resonance [77] or neutron scattering.

To enable a detailed comparison with other crystalline ices, we referred to data from doped hexagonal ice, from ice XII, and from doped structure sII clathrate hydrates. From this compilation, it is clear that the occurrence of a phase transition to an ordered state at a temperature  $T_c$  cannot be associated with a specific dielectric time scale  $\tau$ .

## ACKNOWLEDGMENTS

Support of this project by the Deutsche Forschungsgemeinschaft (DFG) under Grant No. BO1301/12-1 and by the Austrian Science Fund (FWF) under Project I1392 is gratefully acknowledged. V.F.L. is a recipient of a DOC fellowship of the Austrian Academy of Sciences ÖAW at the Institute of Physical Chemistry, University of Innsbruck. We are indebted to Katrin Amann-Winkel for help in the initial stages of the current work.

- 
- [1] P. G. Debenedetti, Supercooled and glassy water, *J. Phys.: Condens. Matter* **15**, R1669 (2003).
  - [2] K. Amann-Winkel, R. Böhmer, C. Gainaru, F. Fujara, B. Geil, and T. Loerting, Colloquium: water's controversial glass transitions, *Rev. Mod. Phys.* **88**, 011002 (2016).
  - [3] V. F. Petrenko and R. W. Whitworth, *Physics of Ice* (University Press, Oxford, 1999).
  - [4] C. Lobban, J. L. Finney, and W. F. Kuhs, The structure of a new phase of ice, *Nature* **391**, 268 (1998).
  - [5] C. G. Salzmann, G. P. Radaelli, A. Hallbrucker, E. Mayer, and J. L. Finney, The preparation and structures of hydrogen ordered phases of ice, *Science* **311**, 1758 (2006).
  - [6] C. G. Salzmann, G. P. Radaelli, E. Mayer, and J. L. Finney, Ice XV: A New Thermodynamically Stable Phase of Ice, *Phys. Rev. Lett.* **103**, 105701 (2009).
  - [7] A. Falenty, T. C. Hansen, and W. F. Kuhs, Formation and properties of ice XVI obtained by emptying a type sII clathrate hydrate, *Nature* **516**, 231 (2014).
  - [8] S. J. L. Placa, W. C. Hamilton, B. Kamb, and A. Prakash, On a nearly proton-ordered structure for ice IX, *J. Chem. Phys.* **58**, 567 (1973).
  - [9] E. Whalley, D. W. Davidson, and J. B. R. Heath, Dielectric properties of ice VII. Ice VIII: a new phase of ice, *J. Chem. Phys.* **45**, 3976 (1966).
  - [10] C. G. Salzmann, P. G. Radaelli, B. Slater, and J. L. Finney, The polymorphism of ice: five unresolved questions, *Phys. Chem. Chem. Phys.* **13**, 18468 (2011).
  - [11] S. Kawada, Dielectric dispersion and phase transition of KOH doped ice, *J. Phys. Soc. Jpn.* **32**, 1442 (1972).
  - [12] T. Matsuo and H. Suga, Calorimetric study of ices  $\text{I}_h$  doped with alkali hydroxides and other impurities, *J. Phys. Colloq.* **48**, C1-477 (1987).
  - [13] S. Kawada and H. Dohata, Dielectric properties on 72 K phase transition of KOH-doped ice, *J. Phys. Soc. Jpn.* **54**, 477 (1985).
  - [14] S. Kawada and K. Shimura, Dielectric studies of RbOH-doped ice and its phase transition, *J. Phys. Soc. Jpn.* **55**, 4485 (1986).

- [15] Y. Tajima, T. Matsuo, and H. Suga, Phase transition in KOH doped hexagonal ice, *Nature* **299**, 810 (1982).
- [16] S. Kawada, Dielectric properties of KOH-doped D<sub>2</sub>O ice, *J. Phys. Soc. Jpn.* **58**, 295 (1989).
- [17] H. Abe and S. Kawada, The dependency of dielectric relaxation time on alkali metal ion (Li<sup>+</sup>, Na<sup>+</sup>, K<sup>+</sup>, Rb<sup>+</sup>) in alkali-hydroxide-doped ice, *J. Phys. Chem. Solids* **52**, 617 (1991).
- [18] H. Suga, Ultra-slow relaxation in ice and related substances, *Proc. Japan Acad. B* **81**, 349 (2005).
- [19] O. Yamamuro, T. Matsuo, and H. Suga, Dielectric study on pure and KOH-doped tetrahydrofuran clathrate hydrates, *J. Incl. Phenom.* **8**, 33 (1990).
- [20] H. Nelson, A. Nowaczyk, C. Gainaru, S. Schildmann, B. Geil, and R. Böhmer, Deuteron nuclear magnetic resonance and dielectric study of host and guest dynamics in KOH doped tetrahydrofuran clathrate hydrate, *Phys. Rev. B* **81**, 224206 (2010).
- [21] O. Yamamuro, N. Kuratomi, T. Matsuo, and H. Suga, Dielectric study of KOH-doped acetone and trimethylene oxide clathrate hydrates, *J. Phys. Chem. Solids* **54**, 229 (1993).
- [22] M. Tyagi and S. S. N. Murthy, Dielectric relaxation in ice and ice clathrates and its connection to the low-temperature phase transition induced by alkali hydroxides as dopants, *J. Phys. Chem. A* **106**, 5072 (2002).
- [23] P. Parkkinen, S. Riikonen, and L. Halonen, Ice XI: not that ferroelectric, *J. Phys. Chem. C* **118**, 26264 (2014).
- [24] M. Ueda, T. Matsuo, and H. Suga, Calorimetric study of proton ordering in hexagonal ice catalyzed by hydrogen fluoride, *J. Phys. Chem. Solids* **43**, 1165 (1982).
- [25] S. Kawada, G. Jin, and M. Abo, Dielectric properties and 110 K anomalies in KOH- and HCl-doped ice single crystals, *J. Phys. Chem. B* **101**, 6223 (1997).
- [26] In Ref. [5] it is mentioned that doping with KOH has no significant effect on the structure of ice V.
- [27] Y. P. Handa, D. D. Klug, and E. Whalley, Phase transitions of ice V and VI, *J. Phys. Colloq.* **48**, C1-435 (1987).
- [28] B. Mincěva-Šukarova, G. Slark, and W. F. Sherman, The Raman spectra of the KOH-doped ice polymorphs: V and VI, *J. Mol. Struct.* **175**, 289 (1988).
- [29] C. G. Salzmann, P. G. Radaelli, J. L. Finney, and E. Mayer, A calorimetric study on the low temperature dynamics of doped ice V and its reversible phase transition to hydrogen ordered ice XIII, *Phys. Chem. Chem. Phys.* **10**, 6313 (2008).
- [30] G. P. Johari and E. Whalley, The dielectric relaxation time of ice V, its partial anti-ferroelectric ordering and the role of Bjerrum defects, *J. Chem. Phys.* **115**, 3274 (2001).
- [31] C. G. Salzmann, A. Hallbrucker, J. L. Finney, and E. Mayer, Raman spectroscopic study of hydrogen ordered ice XIII and of its reversible phase transition to disordered ice V, *Phys. Chem. Chem. Phys.* **8**, 3088 (2006).
- [32] C. Knight and S. J. Singer, Hydrogen bond ordering in ice V and the transition to ice XIII, *J. Chem. Phys.* **129**, 164513 (2008).
- [33] M. Martin-Conde, Computer simulation of two new solid phases of water: ice XIII and ice XIV, *J. Chem. Phys.* **125**, 116101 (2006).
- [34] E. G. Noya, M. M. Conde, and C. Vega, Computing the free energy of molecular solids by the Einstein molecule approach: Ices XIII and XIV, hard-dumbbells and a patchy model of proteins, *J. Chem. Phys.* **129**, 104704 (2008).
- [35] J. E. Bertie, L. D. Calvert, and E. Whalley, Transformations of ice II, ice III, and ice V at atmospheric pressure, *J. Chem. Phys.* **38**, 840 (1963).
- [36] C. G. Salzmann, I. Kohl, T. Loerting, E. Mayer, and A. Hallbrucker, The low-temperature dynamics of recovered ice XII as studied by differential scanning calorimetry: a comparison with ice V, *Phys. Chem. Chem. Phys.* **5**, 3507 (2003).
- [37] C. Sotin and J. P. Poirier, Viscosity of ice V, *J. Phys. Colloq.* **48**, C1-233 (1987).
- [38] W. B. Durham, L. A. Stern, and S. H. Kirby, Rheology of water ices V and VI, *J. Geophys. Res. Solid Earth* **101**, 2989 (1996); W. B. Durham and L. A. Stern, Rheological properties of water ice—applications to satellites of the outer planets, *Annu. Rev. Earth Planet. Sci.* **29**, 295 (2001).
- [39] C. A. Tulk, H. Kieft, M. J. Clouter, and R. E. Gagnon, Elastic constants of ice III, V, and VI by Brillouin spectroscopy, *J. Phys. Chem. B* **101**, 6154 (1997).
- [40] B. Kamb, A. Prakash, and C. Knobler, Structure of ice V, *Acta Cryst.* **22**, 706 (1967).
- [41] W. F. Kuhs, C. Lobban, and J. L. Finney, Partial H-ordering in high pressure ices III and V, *Rev. High Pressure Sci. Technol.* **7**, 1141 (1998).
- [42] C. Lobban, J. L. Finney, and W. F. Kuhs, The structure and ordering of ices III and V, *J. Chem. Phys.* **112**, 7169 (2000).
- [43] J. E. Bertie, H. J. Labbé, and E. Whalley, Far-infrared spectra of ice II, V, and IX, *J. Chem. Phys.* **49**, 775 (1968).
- [44] J. E. Bertie and E. Whalley, Infrared spectra of ices II, III, and V in the range 4000 to 350 cm<sup>-1</sup>, *J. Chem. Phys.* **40**, 1646 (1964).
- [45] M. J. Taylor and E. Whalley, Raman spectra of ices Ih, Ic, II, III, and V, *J. Chem. Phys.* **40**, 1660 (1964).
- [46] B. Mincěva-Šukarova, G. E. Slark, and W. F. Sherman, The Raman spectra of ice V and ice VI and evidence of partial proton ordering at low temperatures, *J. Mol. Struct.* **143**, 87 (1986).
- [47] J.-C. Li, J. D. Londono, D. K. Ross, J. L. Finney, J. Tomkinson, and W. F. Sherman, An inelastic incoherent neutron scattering study of ice II, IX, V, and VI—in the range from 2 to 140 meV, *J. Chem. Phys.* **94**, 6770 (1991).
- [48] R. B. Ayala and V. Tchijov, A molecular dynamics study of ices III and V using TIP4P and TIP5P water models, *Can. J. Phys.* **81**, 11 (2003).
- [49] L. G. MacDowell and C. Vega, Dielectric constant of ice Ih and ice V: a computer simulation study, *J. Phys. Chem. B* **114**, 6089 (2010).
- [50] The ice V sample studied in Ref. [30] was reported to contain “an unknown amount of ice II,” and the possible presence of small impurity molecules (such as N<sub>2</sub> and CO<sub>2</sub>) was raised. The pressure in the dielectric cell used in Ref. [30] was stated to be 3.7 kbar.
- [51] G. J. Wilson, R. K. Chan, D. W. Davidson, and E. Whalley, Dielectric properties of ices II, III, V, and VI, *J. Chem. Phys.* **43**, 2384 (1965).
- [52] G. P. Johari, S. J. Jones, and J. Perez, The orientational correlation tensor in ice-I, ice-III, ice-IV, ice-V, and ice-VI, *Phil. Mag. B* **50**, L1 (1984).
- [53] K. W. Köster, V. Fuentes-Landete, A. Raidt, C. Gainaru, T. Loerting, and R. Böhmer, Dynamics enhanced by HCl doping triggers full Pauling entropy release at the ice XII-XIV transition, *Nat. Commun.* **6**, 7349 (2015).

- [54] K. Amann-Winkel, C. Gainaru, P. H. Handle, M. Seidl, H. Nelson, R. Böhmer, and T. Loerting, Water's second glass transition, *Proc. Nat. Acad. Sci.* **110**, 17720 (2013).
- [55] W. F. Kuhs and M. S. Lehmann, The geometry and orientation of the water molecule in ice Ih, *J. Phys. Colloques* **48**, C1-3 (1987).
- [56] M. I. McMahon, R. J. Nelmes, W. F. Kuhs, R. Dorwarth, R. O. Piltz, and Z. Tun, Geometric effects of deuteration on hydrogen-ordering phase transitions, *Nature* **348**, 317 (1990); K. Röttger, A. Endriss, J. Ihringer, S. Doyle, and W. F. Kuhs, Lattice constants and thermal expansion of H<sub>2</sub>O and D<sub>2</sub>O ice Ih between 10 and 265 K, *Acta Cryst.* **B50**, 644 (1994).
- [57] C. G. Salzmann, E. Mayer, and A. Hallbrucker, Thermal properties of metastable ices IV and XII: comparison, isotope effects and relative stabilities, *Phys. Chem. Chem. Phys.* **6**, 1269 (2004).
- [58] C. Gainaru, A. L. Agapov, V. Fuentes-Landete, K. Amann-Winkel, H. Nelson, K. W. Köster, A. I. Kolesnikov, V. N. Novikov, R. Richert, R. Böhmer, T. Loerting, and A. P. Sokolov, Anomalous large isotope effect in the glass transition of water, *Proc. Natl. Acad. Sci. USA* **111**, 17402 (2014).
- [59] C. G. Salzmann, P. G. Radaelli, A. Hallbrucker, E. Mayer, and J. L. Finney, in *Symposium on the Physics and Chemistry of Ice, Physics and Chemistry of Ice*, edited by W. F. Kuhs (Royal Society of Chemistry, Cambridge, 2007), p. 521–528.
- [60] It is difficult to compare our dielectric relaxation times for pure ice V with those of Ref. [30], in which a dielectric relaxation time of 1.5 s at 133 K was determined at elevated pressures.
- [61] I. M. Hodge, Enthalpy relaxation and recovery in amorphous materials, *J. Non-Cryst. Solids* **169**, 211 (1994).
- [62] The exothermic heat associated with the transition is, depending on cooling rate, only about 50–90% of that of the protonated analog (see Fig. 5(a) in Ref. [29]).
- [63] S. Kawada, A phenomenological interpretation of anomalous quickening of dielectric relaxation by doping of KOH in ice Ih, *J. Phys. Soc. Jpn.* **57**, 3694 (1988).
- [64] S. Kawada, Acceleration of dielectric relaxation by KOH-doping and phase transition in ice Ih, *J. Phys. Chem. Solids*, **50**, 1177 (1989).
- [65] S. Kawada, I. Takei, and H. Abe, Development of a new relaxational process having shortened relaxation time and phase transition in KOH-doped ice single crystal, *J. Phys. Soc. Jpn.* **58**, 54 (1989).
- [66] S. Zaromb and R. Brill, Solid solutions of ice and NH<sub>4</sub>F and their dielectric properties, *J. Chem. Phys.* **43**, 2965 (1965).
- [67] Y. Tajima, T. Matsuo, and H. Suga, Calorimetric study of phase transition in hexagonal ice doped with alkali hydroxides, *J. Phys. Chem. Solids* **45**, 1135 (1984).
- [68] O. Yamamuro, M. Oguni, T. Matsuo, and H. Suga, High-pressure calorimetric study on the ice XI-I<sub>h</sub> transition, *J. Chem. Phys.* **86**, 5137 (1987).
- [69] O. Yamamuro, M. Oguni, T. Matsuo, and H. Suga, Heat capacity and phase transition of tetrahydrofuran clathrate hydrate, *Solid State Commun.* **62**, 289 (1987).
- [70] O. Yamamuro, M. Oguni, T. Matsuo, and H. Suga, Calorimetric study of pure and KOH-doped tetrahydrofuran clathrate hydrate, *J. Phys. Chem. Solids* **49**, 425 (1988).
- [71] O. Yamamuro, T. Matsuo, H. Suga, W. I. F. David, M. Ibberson, and A. J. Leadbetter, A neutron-diffraction study of tetrahydrofuran and acetone clathrate hydrates, *Physica B* **213–214**, 405 (1995).
- [72] A. I. Krivchikov, O. O. Romantsova, and O. A. Korolyuk, The effect of proton ordering on the thermal conductivity of clathrate tetrahydrofuran hydrate, *Low Temp. Phys.* **34**, 648 (2008).
- [73] G. P. Johari, A. Lavergne, and E. Whalley, Dielectric properties of ice VII and VIII and the phase boundary between ice VI and VII, *J. Chem. Phys.* **61**, 4292 (1974).
- [74] K. Kobayashi and H. Yasuda, Phase transition of ice I<sub>c</sub> to ice XI under electron beam irradiation, *Chem. Phys. Lett.* **547**, 9 (2012).
- [75] S. Alavi, R. Susilo, and J. A. Ripmeester, Linking microscopic guest properties to macroscopic observables in clathrate hydrates: Guest host hydrogen bonding, *J. Chem. Phys.* **130**, 174501 (2009).
- [76] An upper limit of the mole fraction of those additional L defects was recently estimated from NH<sub>3</sub> doping experiments to be about  $3 \times 10^{-4}$ , see H. Nelson, A. Ihrig, R. Kahlau, P. Kibies, S. M. Kast, and R. Böhmer, Dielectric and deuteron magnetic resonance studies of guest reorientation and defect dynamics in six clathrate hydrates with ring-type guests, *J. Non-Cryst. Solids* **407**, 431 (2015).
- [77] M. Scheuermann, B. Geil, F. Löw, and F. Fujara, Deuteron spectra, spin-lattice relaxation, and stimulated echoes in ice II, *J. Chem. Phys.* **130**, 024506 (2009).